Marine Geology 265 (2009) 120–129

Contents lists available at ScienceDirect

Marine Geology

journal homepage: www.elsevier.com/locate/margeo

Evaluation of two conflicting paradigms for cohesive sediment deposition

H.K. Ha *, J.P.-Y. Maa

Department of Physical Sciences, Virginia Institute of Marine Science, School of Marine Science, College of William and Mary, Gloucester Point, VA 23062, USA

ARTICLE INFO

Article history:
Received 10 December 2008
Received in revised form 15 June 2009
Accepted 7 July 2009
Available online 16 July 2009

Communicated by D.J.W. Piper

Keywords:
Cohesive sediment
Deposition
Critical bed shear stress
Flume experiment

ABSTRACT

Laboratory experiments using steady flows and simulated tidal flows were conducted to evaluate two conflicting paradigms for cohesive sediment transport: mutually exclusive vs. simultaneous erosion and deposition. Due to the secondary flow and skewed distribution of bed shear stress (τ_b), the deposition space is mostly confined to the inner wall of an annular flume. The area of deposition (or the length of deposition because of the axially symmetrical flow) provides an indicator to determine when deposition at the sediment–water interface starts. The direct observation of deposition stemming from the inner corner suggests that a critical shear stress for deposition ($\tau_{cd} = 0.03$–0.06 Pa) does exist. Changes in deposit length and depth-averaged suspended sediment concentration (SSC) under simulated tidal cycles demonstrate that deposition can happen only in tidal decelerating phases when local τ_b is less than τ_{cd}. The exclusive paradigm incorporated with the correct erosion threshold (τ_{ce}) profile and erosion behavior could explain changes in laboratory- and field-observed depth-averaged SSC under all tidal regimes.

1. Introduction

Understanding erosion and deposition processes of cohesive sediment is important for better management of estuarine and coastal environments. These processes are primarily controlled by the variation in hydrodynamic and sedimentary conditions (Umita et al., 1984; McAnally, 1999). It is generally accepted that the bottom sediment is eroded when the bed shear stress (τ_b) is above a critical value, i.e., the critical bed shear stress for erosion (τ_{ce}) (Krone, 1962, 1993; Sanford and Halka, 1993; Winterwerp and van Kesteren, 2004). But the existence of a critical bed shear stress for deposition (τ_{cd}) is still debatable since there is a distinctive gap among results from laboratory experiments (e.g., Krone, 1962; Lau and Krishnappan, 1994), field measurements (e.g., Sanford and Halka, 1993) and numerical simulations (e.g., Sanford and Halka, 1993; Park et al., 2008). The absence or presence of τ_{cd} in cohesive sediment dynamics generates two opposite paradigms — "exclusive" vs. "simultaneous" erosion and deposition, producing different outcomes such as the variation in SSC, erosion and deposition rates (Table 1). It is noted that τ_b, τ_{ce}, and τ_{cd} are all time-averaged parameters, and the time average used in this study means the average over a time scale that is sufficiently longer than the turbulence fluctuation, but much shorter than the variation in applied tidal force.

The exclusive paradigm (Fig. 1a) suggests that erosion and deposition do not occur at the same time. In other words, erosion from the sediment bed occurs only when τ_b is larger than τ_{ce}, and deposition to the bed occurs only when τ_b drops below τ_{cd}. In general, τ_{ce} is slightly greater than τ_{cd} such that an intermediate range ($\tau_{cd} < \tau_b < \tau_{ce}$) can exist in which neither erosion nor deposition occurs (Dyer, 1986; Sanford and Halka, 1993). This paradigm was derived based on a series of laboratory experiments (e.g., Krone, 1962; Partheniades et al., 1968; Parchure and Mehta, 1985; Lau and Krishnappan, 1994). All of the above conclusions were drawn from interpreting the time series of the best-estimated depth-averaged suspended sediment concentration (SSC). It is noted, however, that there is no direct observation of when "deposition" at the sediment–water interface starts.

In contrast, the simultaneous paradigm (Fig. 1b) allows erosion and deposition to occur at the same time (Sanford and Halka, 1993; Winterwerp, 2006). It implies that deposition exists at all times regardless of τ_b. This paradigm was originally proposed to explain behaviors of non-cohesive sediment. Several researchers (e.g., Lavelle et al., 1984; Bedford et al., 1987; Sanford and Halka, 1993) adopted this concept for cohesive sediment transport and successfully simulated the field-observed SSC in their models, therefore the validity of simultaneous paradigm for cohesive sediment has been claimed. Sanford and Halka (1993), for example, showed poor numerical simulation results in the Chesapeake Bay using the "exclusive paradigm." When changed to the "simultaneous paradigm," they were able to better simulate the field-observed SSC. They also explained that the exclusive logic does not work well in field cases because the natural spatial and temporal

* Corresponding author. Present address: Department of Marine Sciences, University of South Alabama, Dauphin Island Sea Lab., Dauphin Island, AL 36528, USA. Tel.: +1 251 861 7503; fax: +1 251 861 7540.
E-mail addresses: hokyung.ha@gmail.com (H.K. Ha), maa@vims.edu (J.P.-Y. Maa).

0025-3227/$ – see front matter © 2009 Elsevier B.V. All rights reserved.
doi:10.1016/j.margeo.2009.07.001

Table 1
Two conflicting paradigms for erosion and deposition of cohesive sediment.

	Exclusive paradigm	Simultaneous paradigm
Definition	Erosion and deposition will not occur at the same time.	Erosion and deposition will occur simultaneously.
Boundary condition[a]	$\frac{\partial C}{\partial t} = E$ for $\tau_b > \tau_{ce}$ $\frac{\partial C}{\partial t} = D$ for $\tau_b < \tau_{cd}$	$\frac{\partial C}{\partial t} = E - D$
Existence of τ_{ce}	Yes	Yes
Existence of τ_{cd}	Yes ($\tau_{cd} < \tau_{ce}$)	No (continuous deposition)
Deposition rate	$D = w_s C_b\left(1 - \frac{\tau_b}{\tau_{cd}}\right)$ for $\tau_b < \tau_{cd}$ $D = 0$ for $\tau_b > \tau_{cd}$	$D = w_s C_b$
References	Krone (1962); Partheniades et al. (1968); Parchure and Mehta (1985); Lau and Krishnappan (1994)	Sanford and Halka (1993); Winterwerp (2006)

[a] Assuming a horizontally uniform flow and C is the depth-averaged suspended sediment concentration; E: Erosion rate; D: deposition rate; w_s: settling velocity; C_b: near-bed concentration.

variability tends to be minimized in laboratory conditions. As pointed out by Maa et al. (2008), however, it is noted that Sanford and Halka's conclusion was based on the observation of SSC at and above a level of 25 cm above the bed, not including the SSC below that level. This means that what they observed was that the downward flux at 25 cm above the bed always existed and was larger than the upward flux when the tidal current (or τ_b) started to decrease.

The aforementioned conflicts between the two paradigms should be clarified to correctly predict the transport and fate of cohesive sediment in estuarine and coastal areas. To resolve the dispute of conflicting paradigms, direct observation of when and where deposition actually occurs would be preferable. For this reason, Maa et al. (2008) conducted a preliminary laboratory experiment to directly observe the deposition process under steady flows. Their results generally support the "exclusive paradigm," but more extensive experiments are necessary to elucidate depositional behaviors under unsteady flows such as tidal currents. Although some early studies (e.g., Hayter, 1983; Umita et al., 1984; van Leussen and Winterwerp, 1990) also simulated cyclic tidal flows in flumes, their objectives were somewhat different, and thus they did not address the question raised here. Nevertheless, their data were reinterpreted to check the validity of the two conflicting paradigms. New flume experiments with more realistic tidal forces were carried out to evaluate which paradigm has more applicability for correctly interpreting both laboratory- and field-observed deposition processes.

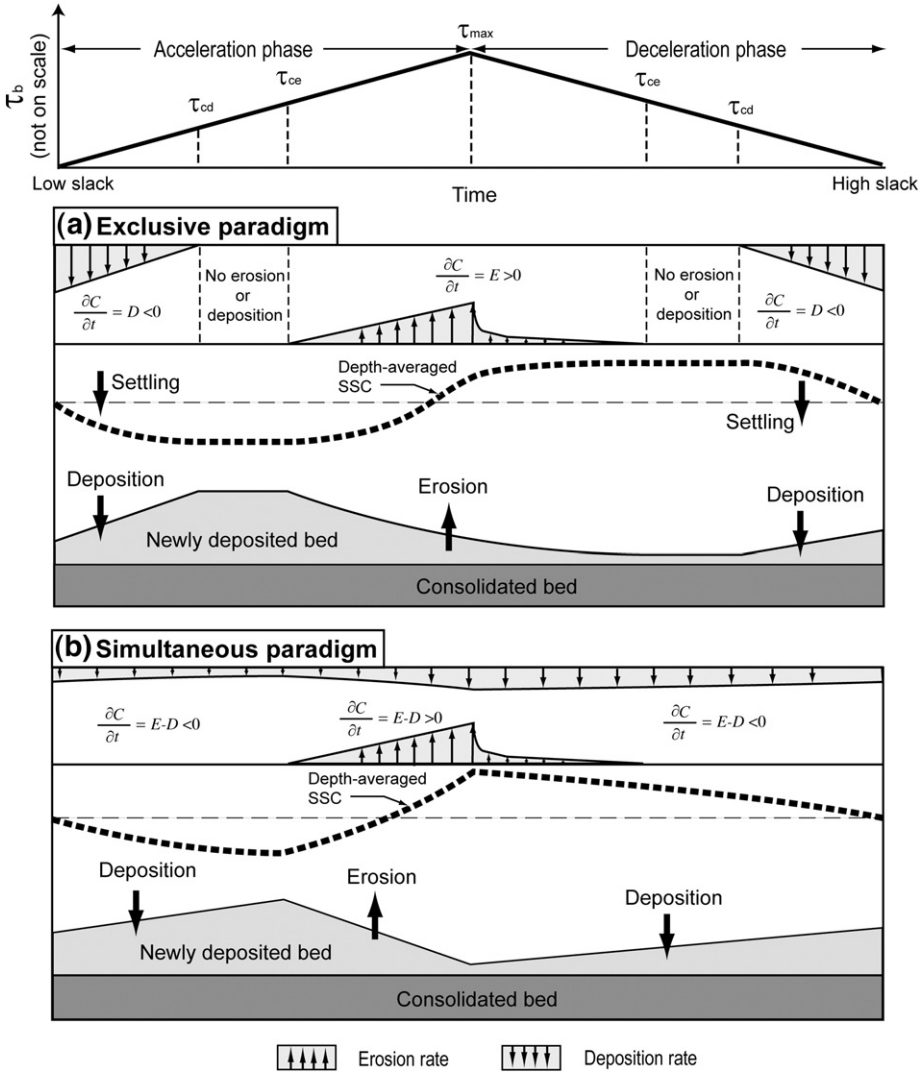

Fig. 1. Conceptual differences between exclusive and simultaneous paradigms for cohesive sediment under tidal forces: (a) exclusive paradigm: erosion from the sediment bed occurs only when $\tau_b > \tau_{ce}$, and deposition to the bed occurs only when $\tau_b < \tau_{cd}$. It is assumed that the new deposit will immediately develop the same τ_{ce}, which does not vary in the vertical direction. The depth-averaged SSC increases whenever $\tau_b > \tau_{ce}$. E and D represent erosion and deposition rate, respectively; and (b) simultaneous paradigm: deposition always exists due to the non-existence of τ_{cd}. The depth-averaged SSC decreases immediately after τ_b starts to decrease because of the continuous deposition regardless of τ_b.

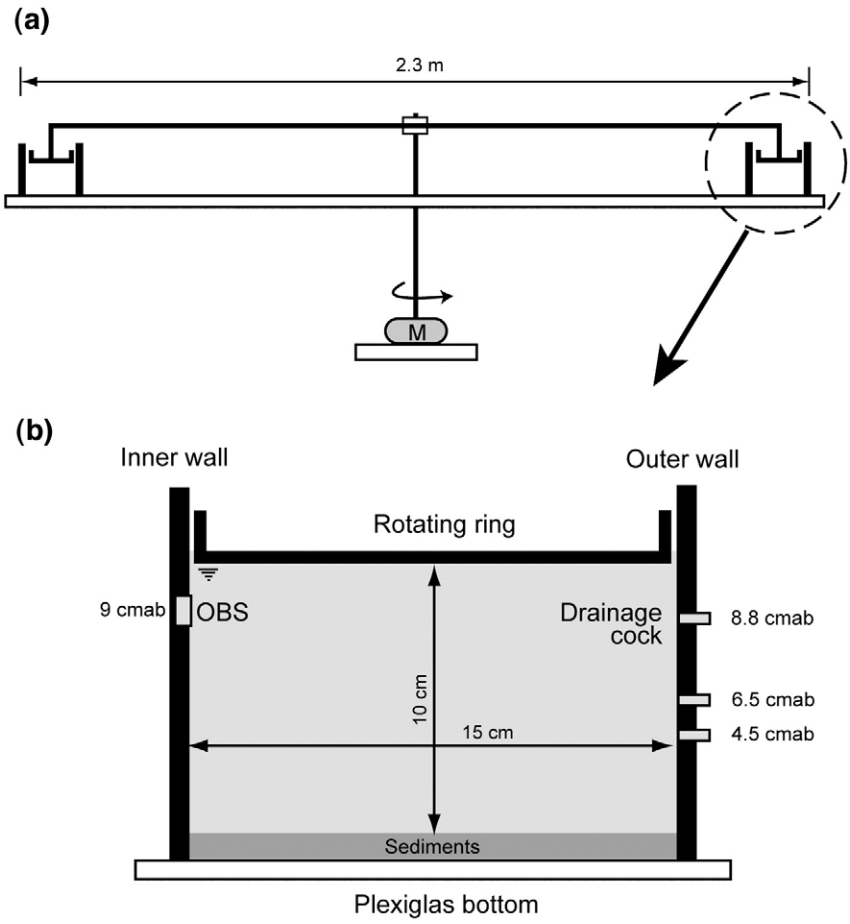

Fig. 2. (a) Schematic diagram of the annular flume housed in the VIMS. M represents a motor. (b) Cross-section view of the flume channel (cmab: cm above bottom).

2. Materials and methods

2.1. Experimental setup

Laboratory experiments were conducted using the annular flume housed in the Virginia Institute of Marine Science (VIMS). The flume has a circular channel with an outer diameter of 2.3 m and a width of 0.15 m (Fig. 2). A top ring driven by an electric motor generated the turbulent flow for eroding bottom sediment. Maa (1993) and Maa et al. (1995) formulated the spatially-averaged bed shear stress, $\langle\tau_b\rangle$, as

$$\langle\tau_b\rangle = 0.0114\Omega^{1.693} \quad (1)$$

where $\langle\tau_b\rangle$ is in Pascal and Ω is the ring speed in rpm. An optical backscatter sensor (OBS) was mounted on the inner wall at 9 cm above the flume bottom to continuously measure the changes in SSC. Due to the relatively strong secondary circulation, suspended sediment was uniformly mixed in the flume. Thus, the readings from a single OBS could represent the depth-averaged SSC. Water temperature in the channel was measured by a thermal sensor. To reduce data noise, each record represents the average of 100 measurements in 7 s. It is noted, therefore, that $\langle\tau_b\rangle$ is a spatially- and temporally-averaged parameter selected for the flume operation. The SSC is also a time- and depth-averaged parameter.

The distribution of τ_b was not uniform across the channel because of the presence of wall effects and the secondary flow induced by the centrifugal force, (Maa, 1993; Maa et al., 1995). Fig. 3 shows τ_b distributions (e.g., τ_{b1}, τ_{b2} and τ_{b3}) for three different $\langle\tau_b\rangle$'s. Due to side-wall effects, τ_b is zero at $r = 1.0$ m (and 1.15 m). Due to the eccentric force, τ_b is relatively larger on the outer half of the flume. Notice that two small areas near both corners, where $\tau_b < \tau_{cd}$, may provide space for sediment deposition, and the area (where τ_b is small) near the inner wall is much larger than that near the outer wall due to the skewed distribution of τ_b (Fig. 3). The flow is axially symmetrical within the VIMS flume, therefore the deposit length ("DL" marked in Fig. 3) represents the depositional area. When $\langle\tau_b\rangle$ is large, DL is small, whereas when $\langle\tau_b\rangle$ is smaller than a certain value (see τ_{b3} in Fig. 3), DL may rapidly increase.

Sediment collected from Mai Po, Hong Kong, was used in all experiments. The median grain size (d_{50}) was 2.6 μm. Clay minerals consisted of kaolinite (51%), smectite (25%) and muscovite (24%).

2.2. Experimental procedure

Prior to the commencement of an experiment, the flume was filled with a sediment–water mixture of a known concentration. Sea salt was added to reach the desired salinity (10 psu). The top ring was lowered into the flume to produce a water depth of 10 cm. The sediment–water mixture was fully mixed again under a large $\langle\tau_b\rangle$ of approximately 1.1 Pa for 24 h. Then, the ring was stopped to allow suspended sediment to deposit and consolidate for 24 h.

Two types of tests (stepwise steady flows and simulated tides) were carried out to reveal depositional behaviors (Table 2). The first type was a repeated experiment to verify the observation by Maa et al. (2008). A large $\langle\tau_b\rangle$ was applied for 1 h, and then the ring rotation speed was sequentially reduced to observe depositional behaviors and the growth of DL (Fig. 4). In the second type, $\langle\tau_b\rangle$ started from zero and linearly increased to a predetermined maximum (0.32 Pa), and then $\langle\tau_b\rangle$ linearly decreased to zero (Figs. 5 and 6). This cycle was repeated three times to monitor the bed response induced by the artificial tides.

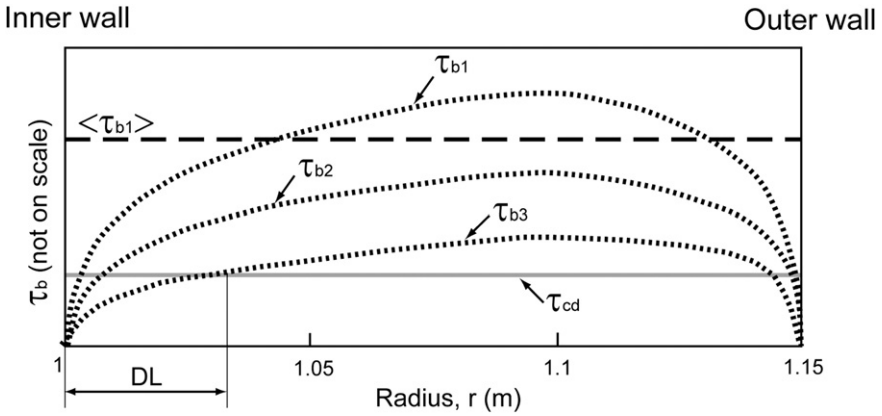

Fig. 3. Distribution of bed shear stress in the annular flume (after Maa, 1993; Maa et al., 2008). $\langle\tau_{b1}\rangle$ is the spatially-averaged bed shear stress for τ_{b1} distribution. τ_{b2} and τ_{b3} show the distribution of two smaller bed shear stresses. DL represents the deposit length near the inner wall.

During the experiment, through the transparent Plexiglas bottom, the growth and decay of DL in the radial direction were observed. Water samples were taken several times through drainage cocks at three different elevations (Fig. 2) for calibrating OBS. Withdrawn samples were filtered through 0.7-μm glass fiber filters. The residues on filters were oven dried at 103–105 °C for 24 h, and then weighed to determine the SSC.

3. Results

3.1. Experiment with stepwise steady bed shear stresses

In this experiment, after $\langle\tau_b\rangle$ was reduced to 0.13 Pa, the duration for each step was changed to 2 h (Fig. 4a). During the entire period of $\langle\tau_b\rangle = 0.13$ and 0.09 Pa, the SSC decreased gently but the DL remained the same (Fig. 4b and c). This may be interpreted by the continuous deposition at the confined space near the inner corner. The decrease in SSC contributed to the increase in mud bed thickness at the deposition area. For the next $\langle\tau_b\rangle$ (i.e., 0.06 Pa), the SSC showed a small drop, and then continued the same decreasing trend. The DL increased to 1.5 cm after about 0.5 h, and remained constant thereafter. In the transition period between $\langle\tau_b\rangle = 0.06$ and 0.03 Pa, the SSC dropped and further decreased from approximately 1.05 to 0.95 g/L (see the arrow in Fig. 4b), whereas the DL sharply increased from 1.5 to 3.3 cm (see the shaded area in Fig. 4c). This sharp increase in DL implies that $\langle\tau_b\rangle$ was close to τ_{cd}, and thus τ_{cd} for the selected sediment was around 0.03 Pa. This result is very close to τ_{cd} ($\approx$0.04 Pa) obtained by Maa et al. (2008).

3.2. Experiment with simulated tidal cycles

For the second experiment, the measurement focused on the change in SSC. The selected maximum bed shear stress $\langle\tau_{max}\rangle$ was approximately 0.32 Pa (Fig. 5a). In the first tidal cycle, there was no noticeable increase in SSC until $\langle\tau_b\rangle$ approached 0.1 Pa, which indicates that τ_{ce} was about 0.1 Pa for this self-weight consolidated bed. When $\langle\tau_b\rangle$ increased to 0.28 Pa in the first tidal cycle, the OBS was saturated, as indicated by the flattened output of OBS that is close to 5 V. Therefore, an SSC that is higher than 0.87 g/L was not used in Fig. 5b. In the slack tide ($\langle\tau_b\rangle = 0$) after the first cycle, there was a clear drop of SSC at the elapsed time of 6.6 h and later at 13.25 h after another tidal cycle (see vertical arrows in Fig. 5c and d).

At the beginning of the second and third tidal acceleration phases, it was noted that the SSC was still gently decreasing (see Fig. 5c and d) although the tidal current was accelerating. A time lag of 0.9 h was observed between minimum $\langle\tau_b\rangle$ (at 6.6 h) and minimum SSC (at 7.5 h), which might be caused by the continuous deposition at the inner corner area during the early stage of the acceleration phase. The SSC showed a small increase at the onset of acceleration (6.7–6.8 h and 13.3–13.4 h) but it immediately decreased again. This response can be explained by the process that the small amount of sediment which was newly deposited near the center of channel during the previous slack tide was easily re-dispersed, but quickly re-deposited at the corner where $\tau_b < \tau_{cd}$. When $\langle\tau_b\rangle$ was sufficiently large (>0.1 Pa), the deposition zone became small, and the newly erodible amount became large enough to produce an increasing SSC again after 7.5 h (and 14.6 h in the third cycle). In order to confirm the OBS-derived SSC, water samples were taken at three different elevations during the early stage of the acceleration phases in the second and third cycles. The sample-derived SSC matched well with the corresponding OBS-derived SSC (Fig. 5c and d). Deposition at the corner, therefore, was still a dominant process even in the early stage of the accelerating phases.

The SSC accordingly increased with $\langle\tau_b\rangle$ until it reached 0.32 Pa. While $\langle\tau_b\rangle$ decreased from 0.32 to 0.15 Pa, the SSC remained nearly constant around 0.5 g/L. When $\langle\tau_b\rangle < 0.15$ Pa, the SSC began to quickly decrease because the deposition zone became sufficiently large.

As the tidal cycle proceeded, the maximum SSC at each cycle gradually decreased (Fig. 5b). This may be associated with the secondary circulation as well as the uneven distribution of τ_b (see Fig. 3). Before running an experiment, the initial thickness of sediment bed was considered uniform across and along the channel, since the sediment–water mixture was naturally settled and consolidated. After one tidal cycle, however, the deposit near the inner wall was thicker than that near the middle of channel where local τ_b is the highest. Once sediment particles (or flocs) were deposited within the deposition zone (where $\tau_b < \tau_{cd}$) under $\langle\tau_{max}\rangle$, it was difficult for those particles (or flocs) to escape from this zone over successive tidal cycles. Also, the relatively strong secondary circulation in the flume continuously brought sediment from high-τ_b area to low-τ_b area near the inner wall. As a result, the erodible sediment on the bed diminished, which led to a decrease in the maximum SSC over the simulated cycles (Fig. 5b). Water sampling during the experiment may have also contributed to the decrease in SSC a little, but it was proven not to be significant by carrying out a control test without any water sampling under the same hydrodynamic conditions. Consequently, the main reason for the decreasing

Table 2
Summary of experimental conditions and results.

	Case 1	Case 2	Case 3
Shear stress type	Stepwise	Tidal cycle	Tidal cycle
$\langle\tau_{max}\rangle$ (Pa)	1.14	0.32	0.32
τ_{cd} (Pa)[a]	0.03	n/a	0.06
Water temperature (°C)	26.5	25.9	27.3
Salinity (psu)	10	10	10
Sediment	Mai Po mud	Mai Po mud	Mai Po mud

[a] Determined by the deposit length near the inner wall.

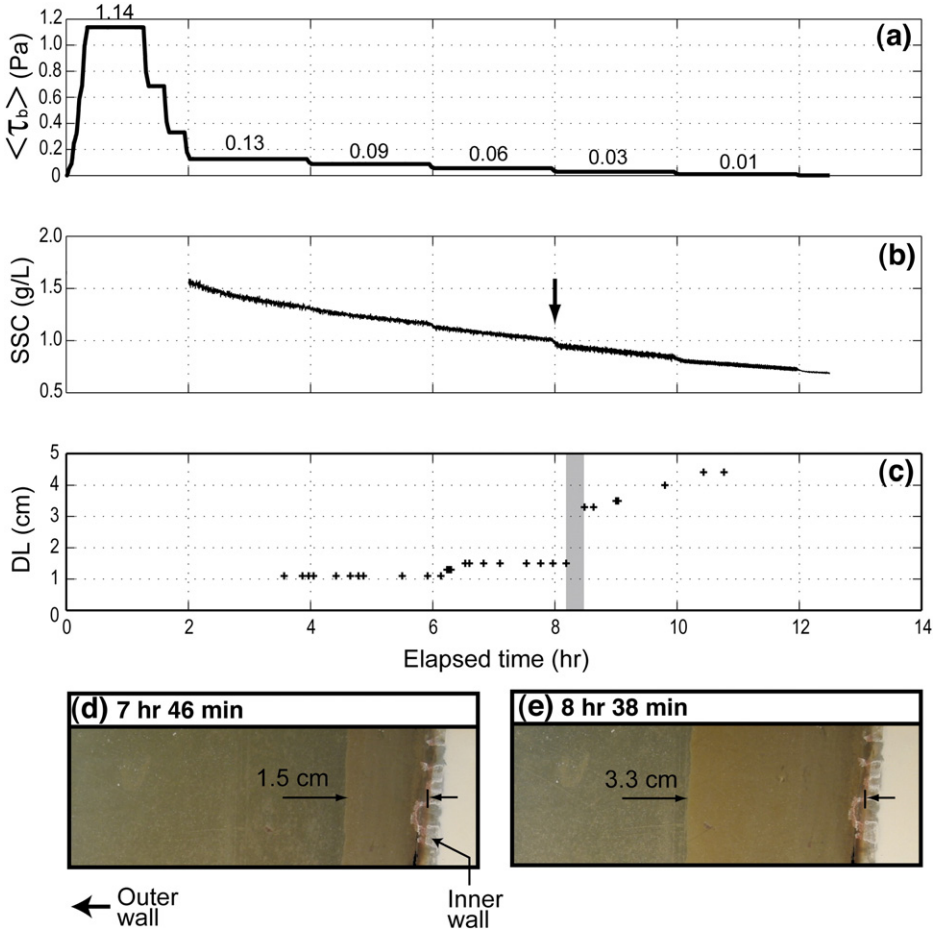

Fig. 4. Experiment results under stepwise steady bed shear stresses (Case 1 in Table 2): (a) $\langle\tau_b\rangle$; (b) OBS-derived SSC; (c) deposit length (DL) accreted near the inner wall; and (d) and (e) are photo images taken from the flume bottom, facing upward, at the elapsed time of 7 h 46 min and 8 h 38 min, respectively.

maximum SSC over repeated cycles was attributed to the secondary flow and the continuous deposition near the inner corner where $\tau_b<\tau_{cd}$.

The third experiment was conducted using the same $\langle\tau_b\rangle$ employed for the second experiment, but with less sediment for bed preparation (Fig. 6). The SSC generally followed a similar trend as shown in Fig. 5, but the maximum SSC was reduced to 0.38 g/L because of less sediment supply from the bed. Thus, the OBS was not saturated and the SSC continued to increase until $\langle\tau_b\rangle$ reached 0.32 Pa. While $\langle\tau_b\rangle$ was reduced

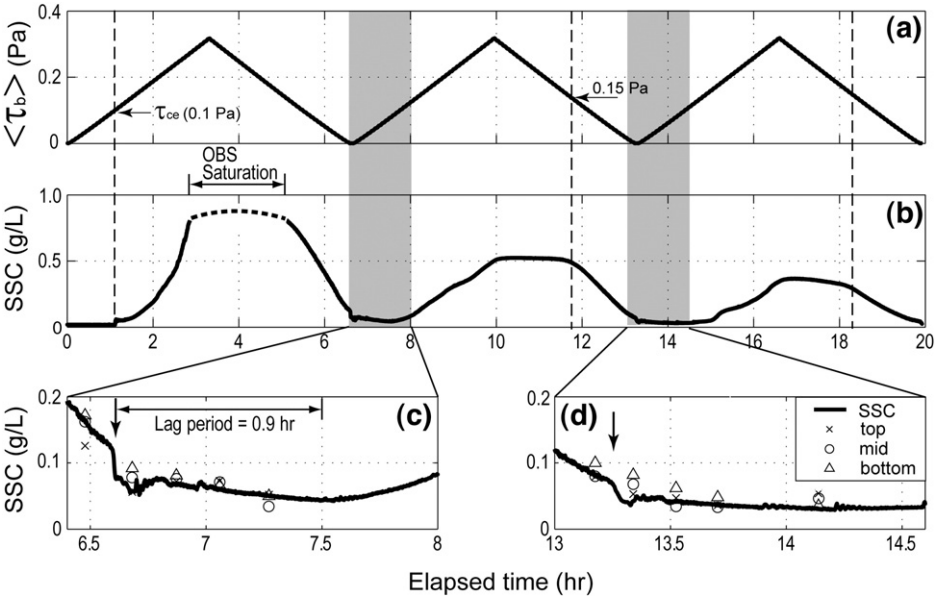

Fig. 5. Experiment results from the first simulated tidal cycles (Case 2 in Table 2): (a) $\langle\tau_b\rangle$; (b) OBS-derived SSC; and (c) and (d) are details of the shaded areas in the second panel. The symbols represent the sample-derived SSCs at three different levels.

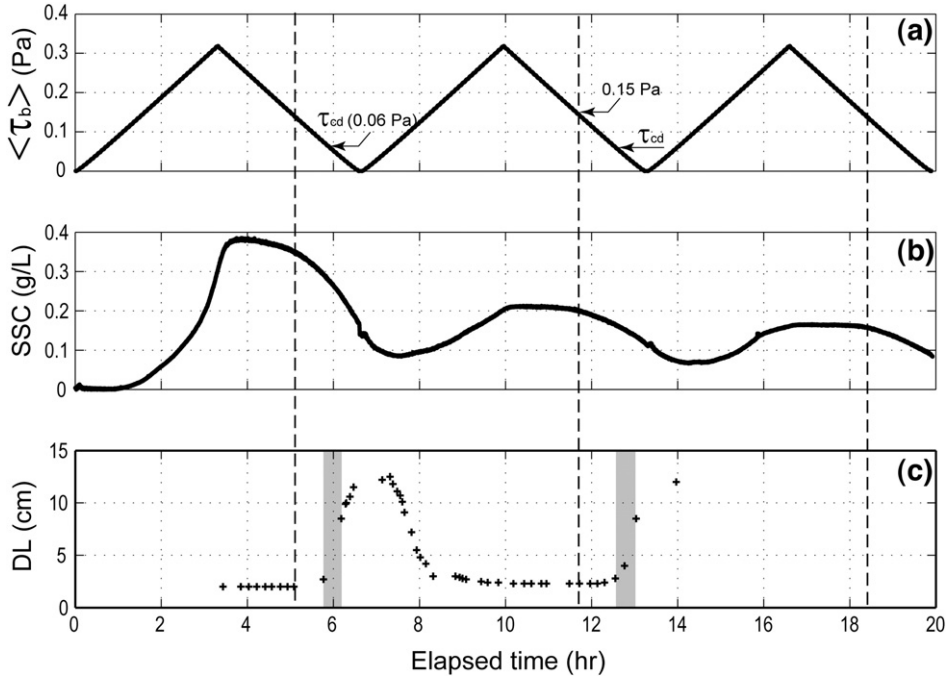

Fig. 6. Experiment results from the second simulated tidal cycles (Case 3 in Table 2): (a) $\langle\tau_b\rangle$; (b) OBS-derived SSC; and (c) deposit length (DL) accreted near the inner wall.

from 0.32 to 0.15 Pa at the early time of deceleration phase, DL remained at 2 cm and SSC continued to slowly decrease (Fig. 6b and c), which implies that deposition occurred at the small area near the inner wall and contributed to the increase in bed thickness in that small area during this period. There was a similar response, i.e., slight decrease in SSC with nearly constant DL when $\langle\tau_b\rangle$ further decreased from 0.15 to 0.06 Pa in the decelerating phase at every cycle. This suggests that the same process was still prevailing during this period. The sharp increase in DL at approximately 5.8 h in the first tidal cycle (and 12.6 h in the second cycle) suggests that $\langle\tau_b\rangle$ was close to τ_{cd} ($\approx$0.06 Pa) (Fig. 6c).

4. Discussion

4.1. Deposition rate vs. downward flux

By definition, deposition is a process by which sediment particles (or flocs) come to the bed and, most importantly, stick to it (Krone, 1993; McAnally, 1999). According to the formula given by Krone (1993), deposition is a function of τ_b, settling velocity and concentration of depositing aggregates. On the other hand, downward flux is defined as the downward movement of sediment particles (or flocs) caused by gravity (McAnally, 1999). The SSC at a practical observation level above the bed can be determined by the competition between downward flux by gravity and upward flux by turbulent diffusion. The advective vertical transport (wC, where w is the vertical component of tidal current and C is the SSC) also contributes to the change in SSC, but its role is not significant because the decrease in SSC happens in both flood ($w>0$) and ebb ($w<0$) tides (Maa et al., 2008). When there is a sufficient sediment supply by bed erosion (e.g., when $\tau_b>\tau_{ce}$ at tidal acceleration phases) and the eddy diffusivity is also strong, the upward diffusion flux would be larger than the downward settling flux. As a result, the SSC at the observation elevation would increase with time. In contrast, if there is no sediment supply when erosion stops (e.g., when $\tau_b<\tau_{ce}$ at tidal deceleration phases and slack tides), the upward flux may be smaller than the downward flux. As such, the SSC would decrease at the observation level. The above description suggests that the decrease in SSC at a specified distance above the bed may not be always caused by deposition. This is because the net downward flux would form a relatively high-concentration layer (so called "buffer layer") right above the bed but the sediment particles still remain in suspension. In this study, such a buffer layer cannot exist because of the presence of a strong secondary circulation. In a field site or a flume without secondary circulation, however, this layer would frequently form and move with the mean current. For this reason, its forming process cannot be treated as deposition. Consequently, the question as to whether deposition actually occurs or not should be dealt with directly at the bed, not in the water column with the change of SSC. The only valid alternative would be using the true total SSC or the true depth-averaged SSC under the condition that the near-bed SSC can be measured accurately.

4.2. Secondary circulation effect

Previous laboratory studies (e.g., Hayter, 1983; Umita et al., 1984; van Leussen and Winterwerp, 1990) that used the simulated tides ($T\approx$12 h) were compared with the results of this study to reveal the effect of secondary circulation (Table 3 and Fig. 7). Although SSC responses are different due to differences in flume dimensions, experimental conditions and selected sediment, this comparison is valuable for understanding cohesive sediment behaviors with a strong or a weak secondary circulation. All previous studies used annular flumes which have the channel and the ring rotating in opposite directions to minimize the secondary flow.

Interestingly, previous works showed that the maximum SSC slightly increased with the number of tidal cycles although they used a constant $\langle\tau_{max}\rangle$. The increasing trend is not clearly shown in Fig. 7 because only two tidal cycles were displayed, but it was reported in those studies. This outcome is likely when the secondary flow was weakened by rotating the channel and the ring in opposite directions.

When the secondary circulation is negligible, the new top layer deposited during the slack period after the first tidal cycle will be uniformly distributed across the channel. The newly deposited materials would be easily agitated and eroded when the tidal current accelerates again. Compared with previous cycles, the bed right below this new layer would be exposed to the fluid shear earlier, so that more sediment could be eroded even if the duration of erosion and $\langle\tau_{max}\rangle$ remain the same. This is possible because of the nature of turbulent flow. Under turbulent flows, although $\langle\tau_{max}\rangle$ is the same, there are always short bursts with instantaneous bed shear stress that is greater than $\langle\tau_{max}\rangle$.

Table 3
Comparison of annular flume experiments with artificial tidal cycles.

	Hayter (1983)	Umita et al. (1984)	van Leussen and Winterwerp (1990)	This study
$\langle\tau_{max}\rangle$ (or max. velocity)	0.5 m/s	0.4 Pa	0.4 Pa	0.32 Pa
Flume outer diameter (m)	1.73	2.2	2.1	2.3
Water depth (m)	0.3	0.2	0.3	0.1
Channel width (m)	0.21	0.2	0.2	0.15
Ratio of width/depth	0.7	1.0	0.67	1.5
Salinity (psu)	10	n/a	n/a (salt water)	10
Water temperature (°C)	n/a	20	n/a	26.6
In phase of $\langle\tau_b\rangle$ and SSC	Yes	No	No	No
d_{50} of sediment (μm)	n/a	6	n/a	2.6
Sediment source	Clay from Lake Francis	Clay and silt from River Chikugo	Commercial kaolinite	Clay from Mai Po wetland
Consolidation time (h)	40	24	n/a	24
Channel and ring rotation	Opposite rotation	Opposite rotation	Opposite rotation	Only ring rotation

The repetition of tidal cycles, therefore, can produce more erosion and gradually increase the SSC. This process may be responsible for the "weakening process" in the sediment bed claimed by van Leussen and Winterwerp (1990). They showed that the maximum SSC in the 27th tidal cycle was about three times higher than that in the 1st cycle, and explained that the slow increasing trend over tidal cycles was caused by the increase in bed erosion rate.

On the other hand, our experimental results showed that the maximum SSC decreased with tidal cycles (Fig. 7d), due to the reason explained in the previous section. Once deposited near the inner wall, the chance for resuspension would be small, and thus the decreasing trend was observed.

In order to demonstrate these two kinds of SSC-response patterns under simulated tidal cycles, the conceptual diagram given by Umita et al. (1984) was modified based on the strength of secondary circulation in the annular flume (Fig. 8). It is assumed that (1) flood and ebb tidal flows are symmetrical; and (2) the gradient of horizontal advection is zero.

In the case with a weak secondary circulation, the maximum SSC has an increasing trend over tidal cycles (Fig. 8a). During the first accelerating phase, the SSC starts to increase while $\langle\tau_b\rangle$ is approaching τ_{ce}, and then continues to increase until it reaches $\langle\tau_{max}\rangle$. After that, the SSC decreases slightly before $\langle\tau_b\rangle$ approaches τ_{cd}. This small decrease is caused by deposition at the corner areas. A rapid drop of SSC occurs when $\langle\tau_b\rangle$ approaches τ_{cd}, and then a new deposition layer is uniformly developed above the old bed. When $0<\langle\tau_b\rangle<\tau_{cd}$ in the next tidal acceleration phase, deposition still continues, but re-dispersion of newly deposited materials, which have a negligibly small τ_{ce}, also starts. As a result, the SSC may increase immediately, and a rapid increase in SSC might be observed before $\langle\tau_b\rangle$ reaches τ_{ce}.

In the case with a strong secondary circulation like the VIMS carousel (Fig. 8b), the first tidal cycle produced the similar SSC response when compared with the former case. When $0<\langle\tau_b\rangle<\tau_{cd}$ in the first deceleration phase, the amount of sediment deposited near the corner area would be larger than that for the previous case because the secondary circulation continues to bring sediment to the deposition area. When $0<\langle\tau_b\rangle<\tau_{cd}$ in the next acceleration phase, deposition is still dominant because the dispersible materials (produced from the high-τ_b area) would deposit at the low-τ_b area near the corner. Thus, the decreasing period of SSC at the early stage of the second tidal acceleration phase is relatively longer, and the SSC may remain low until $\langle\tau_b\rangle$ reaches τ_{ce}. At that time, a sharp increase in SSC can be generally found. During the following cycles, the secondary flow would continuously bring sediment to the inner wall and deposit it there. Therefore, the second maximum SSC is lower than the first one, and the following tidal cycles show a similar response pattern.

4.3. Paradigm evaluation

The flume used in this study has the spatial variability in τ_b distribution, which is clearly shown in the observation of DL. Nonetheless, the variation in time-averaged SSC will be focused on in this section because other early studies (i.e., Hayter, 1983; Umita et al., 1984; van Leussen and Winterwerp, 1990) did not provide any data interpretation on temporal variability.

Hayter (1983) showed that the measured SSC is nearly in phase with flow velocity (Fig. 7a), i.e., the SSC decreased immediately after the flow velocity (or $\langle\tau_b\rangle$) started to decrease and kept the decreasing trend until the next acceleration phase. His result is similar to other field-observed data showing that the SSC increases and decreases in phase with flow velocity (or $\langle\tau_b\rangle$) (e.g., Nichols, 1986; Sanford and Halka, 1993; Maa and

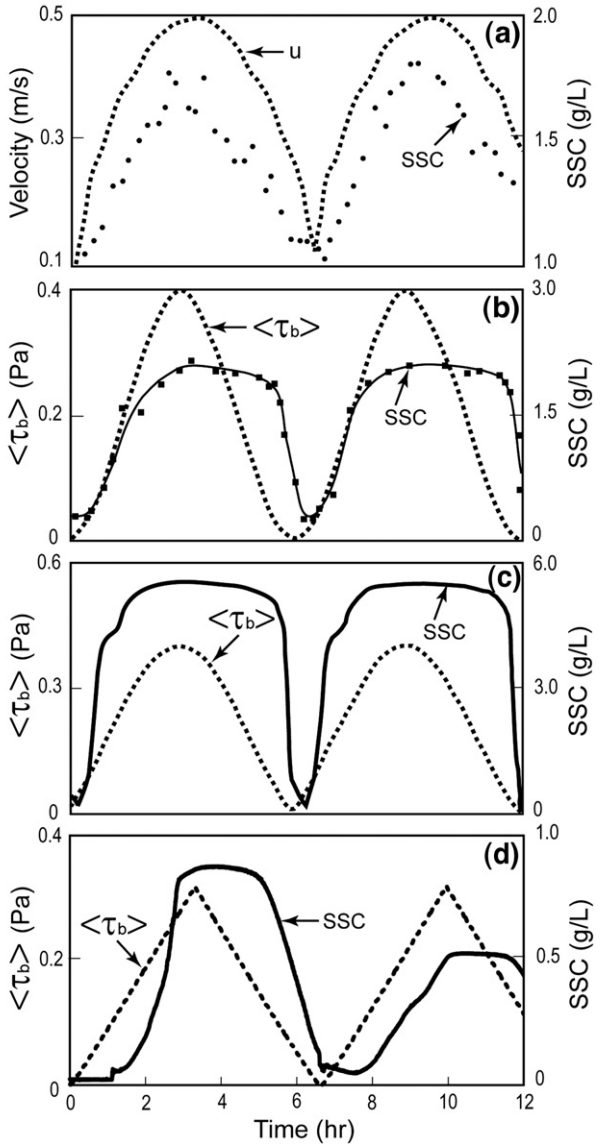

Fig. 7. Comparison of the SSC responses in different studies that simulated tidal cycles: (a) Hayter (1983); (b) Umita et al. (1984); (c) van Leussen and Winterwerp (1990); and (d) this study. The first three studies used an annular flume with both the ring and the channel rotating in opposite directions.

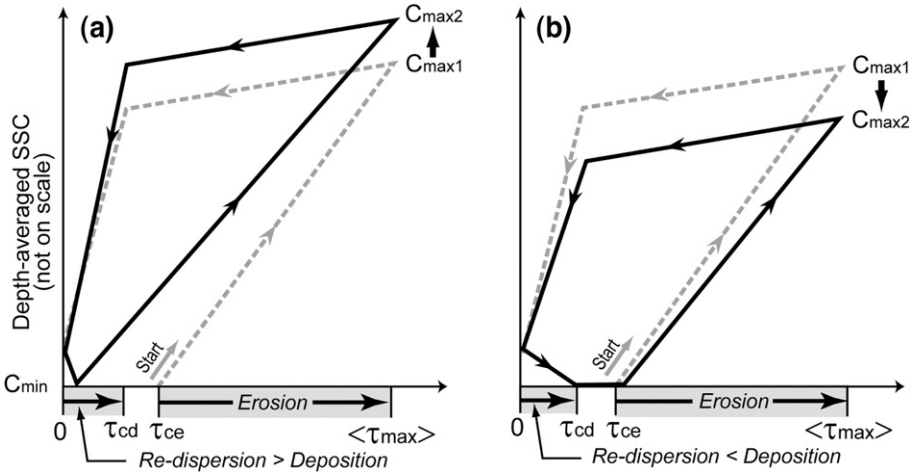

Fig. 8. Two kinds of SSC-response patterns generated by simulated tidal cycles (after Umita et al., 1984): (a) in the flume with a weak secondary circulation; and (b) in the VIMS laboratory carousel with a strong secondary circulation. C_{min} and C_{max} represent the minimum and the maximum SSC, respectively.

Kim, 2002). It is noteworthy, however, that there was no slack period due to the difficulty in flume control. The given minimum velocity was approximately 0.1 m/s which is still strong enough to sustain some sediment particles (or flocs) in suspension. Because there was little secondary circulation to make the SSC uniform in Hayter's flume, the observation represents the local SSC, not the depth-averaged SSC. That is, the phenomena observed during the decelerating phase can be explained by the fact that the downward flux exceeded the upward flux at the sampling elevation. This net downward flux may either (1) develop a near-bed layer with a relatively high SSC when $\langle\tau_b\rangle > \tau_{cd}$ and then deposit when $\langle\tau_b\rangle < \tau_{cd}$ or (2) directly deposit to the bed at all times. Unfortunately, there is no data to support any of these two possibilities.

In contrast, the SSC variation in the latter three data sets (Fig. 7b, c and d) was not in phase with $\langle\tau_b\rangle$. Umita et al. (1984) and van Leussen and Winterwerp (1990) applied the same $\langle\tau_{max}\rangle$ to simulate artificial tidal cycles, and the SSC response showed the similar pattern (see Fig. 7b and c). After $\langle\tau_{max}\rangle$, the SSC remained constant or slightly decreased, and the rapid decrease in SSC was commonly found prior to the slack tides. Umita et al. (1984) observed that floc size was minimized ($d_{50} = 12$ μm) at $\langle\tau_{max}\rangle$ and was maximized ($d_{50} = 31$ μm) immediately before τ_{cd} (≈ 0.025 Pa). They claimed, therefore, that significant deposition started when floc size increased to 31 μm, resulting in the decrease in SSC while $\langle\tau_b\rangle$ was approaching τ_{cd}. Nonetheless, an unanswered question remains: why did the floc size sharply increase immediately before τ_{cd}? In general, it is accepted that floc size is controlled by turbulence which is correlated to $\langle\tau_b\rangle$. The floc size should decrease with decreasing $\langle\tau_b\rangle$, when $\langle\tau_b\rangle$ is lower than about 0.3–0.4 Pa (Manning and Dyer, 2007; Manning et al., 2007), not as claimed by Umita et al. (1984) to have a sudden increase when $\langle\tau_b\rangle$ was close to τ_{cd}. It is worthwhile to point out that the floc size increased from 12 to 31 μm but the effective density of flocs may decrease, so that the increment of settling velocity may not be significant (on the order of 10^{-2} mm/s; Winterwerp and van Kesteren, 2004). Also, the floc sizes (i.e., 12–31 μm) mentioned are very small when compared to real estuarine flocs ranging between 50 μm to a few millimeters (Manning and Dyer, 2007). The observed small change in floc size, therefore, may be difficult to directly link to deposition.

At present, it is not clear what caused the discrepancy in SSC responses between Hayter's experiment (Fig. 7a) and Umita et al. (1984) and van Leussen and Winterwerp's (1990) experiments (Fig. 7b and c), even though all three experiments had rotated the channel and the ring in opposite directions to minimize the secondary flow. One possible explanation is that the secondary circulation in Umita et al. (1984) and van Leussen and Winterwerp's (1990) flumes might not be as weak as that in Hayter's flume. Thus, their measured SSC may closely represent the true depth-averaged SSC.

When there is no secondary circulation, as happens in most field cases, re-dispersion is considered as an important process to provide the sediment supply near the sediment–water interface at the beginning of acceleration phases (Kwon, 2005). Because the fresh sediment deposited during the previous slack tide may only have a short time (1–2 h) to be consolidated, τ_{ce} for this new deposit is small and close to zero (Maa and Kim, 2002). This leads to a quick re-dispersion into the water column, even when τ_b is lower than the typically-accepted τ_{ce} (e.g., about 0.1 Pa). As a result, the SSC starts to increase immediately once the tidal current starts to accelerate (Figs. 8a and 9). This explanation in terms of re-dispersion is in line with other in-situ measurements. Maa and Kim (2002) showed that SSCs measured at 10 cm and 140 cm above the York River bed rapidly increased when the tidal current switched from slack to flood or ebb, not waiting until τ_b reached τ_{ce}. Nakagawa (2005) also presented the variation in near-bed (20 and 50 cm above the bed) SSC in Ariake Bay showing a prompt increase in SSC at the onset of tidal acceleration. These measurements support the view that the newly deposited fluffy sediment is a main source of increase in the near-bed SSC during the early stage of the acceleration phases.

Re-dispersion, however, is gradually shifted to erosion as the tidal acceleration proceeds. Because of the difficulty in accurately estimating the sediment amount by re-dispersion or erosion, Maa and Kim (2002) proposed a simplification of this complicated process using a constant erosion rate (see the dot-dashed line in Fig. 9). They suggested that erosion occurs only when the tidal current is in the acceleration phase. This is a practical approach because the total amount of erodible sediment using the constant erosion rate model may not be significantly different with that using the traditional erosion model in which one has to frequently estimate $\tau_{ce}(z)$, where z is a bed depth, for different stages of consolidations. Using the constant erosion rate estimated from in-situ erosion tests, for example, Kwon et al. (2005) can successfully simulate suspended sediment transport for the York River system.

In the decelerating phase, because erosion ceases and the mixing capacity decreases, a much weak upward transport would be resulted, and thus a net downward flux of suspended sediment is dominant. As a consequence, a relatively high-concentration layer can be formed right above the sediment bed. This can cause the collapse of turbulence, resulting in the super-saturated conditions in terms of carrying capacity (Toorman, 2002; Winterwerp, 2002). Even if the total amount of suspended sediment is still below the saturation concentration, the decelerating flow will not directly induce deposition because the sediment that was already suspended can be maintained in suspension by τ_b that is actually smaller than that required for bed erosion (Masselink and Hughes, 2003). During the early stage of decelerating

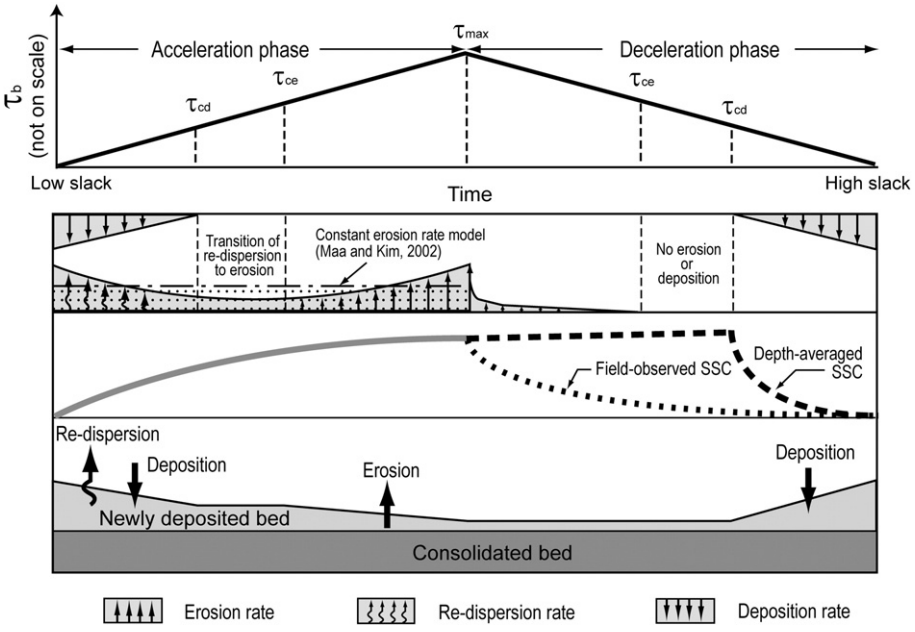

Fig. 9. Revised conceptual diagram showing the near-bed exchange processes of cohesive sediment under tidal cycles. The field-observed SSC at a fixed point (i.e., local SSC and not close to the bottom) in water column can decrease immediately after τ_{max} because of the net downward flux, while the true depth-averaged SSC starts to decrease only when $\tau_b < \tau_{cd}$.

phases, therefore, sediment particles (or flocs) in suspension will only be re-distributed in the water column. The total mass of suspended sediment would not significantly change even though the density and size distribution of particles (or flocs) can be altered by the flocculation process. The depth-averaged SSC, therefore, remains nearly constant in the decelerating period of $\tau_{cd} < \tau_b < \tau_{max}$ (see the dashed line in Fig. 9). During this time, the downward flux continues to bring suspended sediment to the near-bed layer but may not allow to form the sediment bed because τ_b is still too high for deposition. Once τ_b falls below τ_{cd}, the suspended sediment accumulated at the near-bed layer starts deposition, which results in a rapid decrease in the depth-averaged SSC (see Fig. 9). Field-observed SSC (see the dotted line in Fig. 9) at a fixed level above the bed may show the immediate decrease after τ_{max} because the downward sediment flux is more than the upward sediment flux. This is associated with the cut-off of sediment supply from bed and the decrease in vertical advection. The decreasing trend in field-observed SSC would be continued throughout the decelerating phases.

In summary, the gap between the true depth-averaged SSC and the field-observed depth-averaged SSC is attributed to the lack of near-bed SSC information, not to deposition. The change in DL in laboratory studies as well as the reinterpretation of SSC data from previous studies generally supports the "exclusive paradigm."

5. Conclusions

The followings are summarized from this study:

(1) The duplicated steady flow experiment demonstrates that the similar τ_{cd} can be obtained. This confirmed the results of a previous study given by Maa et al. (2008).
(2) Due to the uneven and skewed distribution of local τ_b, the change in DL in the radial direction is direct observation on τ_b distribution in the annular flume. It also serves as direct evidence to find "when and where the suspended sediment can be actually deposited."
(3) Under simulated tidal flows, τ_{cd} can be identified by the rapid increase in DL and the sharp decrease in depth-averaged SSC. Even though DL was measured and interpreted subjectively at discrete times, it can be reasonably concluded that τ_{cd} for the selected sediment was approximately 0.03–0.06 Pa.
(4) Artificial tidal flow experiments support the existence of τ_{cd}. The exclusive paradigm with the correct τ_{ce} profile and erosion behavior could explain changes in laboratory- and field-observed depth-averaged SSC under all tidal regimes.
(5) Deposition only occurs in tidal decelerating phases when the local τ_b is less than τ_{cd}.
(6) Secondary flow in the VIMS carousel is a major contributor to the long-term decrease in maximum SSC over tidal cycles.

Acknowledgements

This work is partly based on the first author's Ph.D. dissertation. C.T. Friedrichs (VIMS) provided helpful comments on an earlier version of this manuscript. L. Morse and K. Weis carefully proofread this manuscript. We also thank two anonymous reviewers for constructive reviews and the editor for helpful editorial comments.

References

Bedford, K.W., Wai, O., Libicki, C.M., van Evra, R., 1987. Sediment entrainment and deposition measurements in Long Island Sound. J. Hydraul. Eng. 113, 1325–1343.
Dyer, K.R., 1986. Coastal Estuarine Sediment Dynamics. John Wiley and Sons, New York. 342 pp.
Hayter, E.J., 1983. Prediction of cohesive sediment transport in estuarine waters. Ph.D. dissertation, University of Florida, 349 pp.
Krone, R.B., 1962. Flume studies of the transport of sediment in estuarial shoaling processes. Final Report, Hydraulic Engineering Laboratory and Sanitary Engineering Research Laboratory, University of California, Berkeley. 110 pp.
Krone, R.B., 1993. Sedimentation revisited. In: Mehta, A.J. (Ed.), Nearshore and Estuarine Cohesive Sediment Transport. AGU, Washington D.C., pp. 108–125.
Kwon, J.-I., 2005. Simulation of turbidity maximums in the York River, Virginia. Ph.D. dissertation, College of William and Mary, 127 pp.
Kwon, J.-I., Maa, J.P.-Y., Lee, D.-Y., 2005. A preliminary implication of the constant erosion rate model to simulate turbidity maximum in the York River, Virginia, USA. In: Maa, J.P.-Y., Sanford, L.P., Schoellhamer, D.H. (Eds.), Estuarine and Coastal Fine Sediments Dynamics. Elsevier, Amsterdam, pp. 331–354.
Lau, Y.L., Krishnappan, B.G., 1994. Does reentrainment occur during cohesive sediment settling? J. Hydraul. Eng. 120 (2), 236–244.
Lavelle, J.W., Mofjeld, H.O., Baker, E.T., 1984. An in situ erosion rate for a fine-grained marine sediment. Journal of Geophysical Research 89, 6543–6552.
Maa, J.P.-Y., 1993. VIMS sea carousel: its hydrodynamic characteristics. In: Mehta, A.J. (Ed.), Nearshore and Estuarine Cohesive Sediment Transport. AGU, Washington D.C., pp. 265–280.
Maa, J.P.-Y., Kim, S.-C., 2002. A constant erosion rate model for fine sediment in the York River, Virginia. Environ. Fluid Mech. 1, 345–360.

Maa, J.P.-Y., Lee, C.-H., Chen, F.J., 1995. Bed shear stress measurements for VIMS Sea Carousel. Mar. Geol. 129, 129–136.
Maa, J.P.-Y, Kwon, J.-I., Hwang, K.-N., Ha, H.-K., 2008. Critical bed shear stress for cohesive sediment deposition under steady flows. J. Hydraul. Eng. 134 (12), 1767–1771.
Manning, A.J., Dyer, K.R., 2007. Mass settling flux of fine sediments in Northern European estuaries: measurements and predictions. Mar. Geol. 245 (1–4), 107–122.
Manning, A.J., Friend, P.L., Prowse, N., Amos, C.L., 2007. Estuarine mud flocculation properties determined using an annular mini-flume and the LabSFLOC system. Cont. Shelf Res. 27, 1080–1095.
Masselink, G., Hughes, M.G., 2003. Introduction to Coastal Processes and Geomorphology. Hodder Arnold, London. 354 pp.
McAnally, W.H., 1999. Aggregation and deposition of estuarial fine sediment. Ph.D. dissertation, University of Florida, 366 pp.
Nakagawa, Y., 2005. Fine sediment transport in Ariake Bay, Japan. In: Maa, J.P.-Y., Sanford, L.P., Schoellhamer, D.H. (Eds.), Estuarine and Coastal Fine Sediments Dynamics. Elsevier, Amsterdam, pp. 377–394.
Nichols, M.M., 1986. Effects of fine sediment resuspension in estuaries. In: Mehta, A.J. (Ed.), Estuarine Cohesive Sediment Dynamics. Springer-Verlag, New York, pp. 5–42.
Parchure, T.M., Mehta, A.J., 1985. Erosion of soft cohesive sediment deposits. J. Hydraul. Eng. 111 (10), 1308–1326.
Park, K., Wang, H.V., Kim, S.-C., Oh, J.-H., 2008. A model study of the estuarine turbidity maximum along the main channel of the upper Chesapeake Bay. Estuar. Coasts 31, 115–133.
Partheniades, E., Cross, R.H., Ayora, A., 1968. Further research on the deposition of cohesive sediments. Proceedings of the 11th Conference on Coastal Engineering, pp. 723–772.
Sanford, L.P., Halka, J.P., 1993. Assessing the paradigm of mutually exclusive erosion and deposition of mud with examples from upper Chesapeake Bay. Mar. Geol. 114, 37–57.
Toorman, E.A., 2002. Modelling of turbulent flow with suspended cohesive sediment. In: Winterwerp, J.C., Kranenburg, C. (Eds.), Fine Sediment Dynamics in the Marine Environment. Elsevier, Amsterdam, pp. 155–169.
Umita, T., Kusuda, T., Awaya, Y., Onuma, M., Futawatari, T., 1984. The behavior of suspended sediments and muds in an estuary. Water Sci. Technol. 17, 915–927.
van Leussen, W., Winterwerp, J.C., 1990. Laboratory experiments on sedimentation of fine-grained sediments: a state-of-the-art review in the light of experiments with the Delft tidal flume. In: Cheng, R.T. (Ed.), Residual Currents and Long-term Transport. Springer-Verlag, New York, pp. 241–259.
Winterwerp, J.C., 2002. Scaling parameters for high-concentrated mud suspensions in tidal flow. In: Winterwerp, J.C., Kranenburg, C. (Eds.), Fine Sediment Dynamics in the Marine Environment. Elsevier, Amsterdam, pp. 171–186.
Winterwerp, J.C., 2006. On the sedimentation rate of cohesive sediment. In: Maa, J.P.-Y., Sanford, L.P., Schoellhamer, D.H. (Eds.), Estuarine and Coastal Fine Sediment Dynamics. Elsevier, Amsterdam, pp. 209–226.
Winterwerp, J.C., van Kesteren, W.G.M., 2004. Introduction to the Physics of Cohesive Sediment in the Marine Environment. Elsevier, Amsterdam. 466 pp.